

Simulation of piezoresistivity in *n*-type single-crystal silicon on the basis of the first-principles band structure

Koichi Nakamura*

Office of Science and Engineering Research, Ritsumeikan University, Kusatsu, Shiga 525-8577, Japan

Yoshitada Isono

Department of Mechanical Engineering, Kobe University, Kobe 657-8501, Japan

Toshiyuki Toriyama

Department of Micro System Technology, Ritsumeikan University, Kusatsu, Shiga 525-8577, Japan

Susumu Sugiyama

Ritsumeikan Global Innovation Research Organization, Ritsumeikan University, Kusatsu, Shiga 525-8577, Japan

(Received 11 March 2009; revised manuscript received 26 May 2009; published 13 July 2009)

We have simulated the piezoresistivity in *n*-type single-crystal bulk silicon based on the first-principles electronic band structure of model structures. Our simple procedure to calculate the piezoresistance coefficients is valid qualitatively and quantitatively for carrier electron transport in the multivalley conduction-band structure of *n*-type bulk silicon; the primitive longitudinal and transverse piezoresistance coefficients originate from the energy gap between the valleys, whereas the shear piezoresistance coefficient π_{44} arises from a distortion of the band energy surface in the valleys and can be presented clearly as a negative constant. The distinction between the origins of longitudinal, transverse, and shear piezoresistivity can be followed as a dependence on a carrier concentration or temperature.

DOI: [10.1103/PhysRevB.80.045205](https://doi.org/10.1103/PhysRevB.80.045205)

PACS number(s): 72.20.Fr, 72.80.Cw, 71.20.Mq

I. INTRODUCTION

Since Smith discovered the piezoresistive effect of semiconductors,¹ stress response to electric properties in single-crystal silicon has been extensively investigated by experimental²⁻¹⁴ and theoretical^{2-4,15-35} analyses. Progress in integrated circuit processes has been advanced with improvement of the piezoresistive sensors fabricated by silicon, and a more qualitative and quantitative estimate of the piezoresistive effect of silicon materials will be indispensable for future development of new micro-electro-mechanical system (MEMS) or nano-electro-mechanical system (NEMS) sensors.

In the conventional semiconductor theory, deformation of the electronic energy band due to stress/strain has been qualitatively given for bulk silicon, and then formulas of the longitudinal and transverse piezoresistance coefficients have been presented by using the deformation potentials of the electronic energy band.^{2-4,15-22,36} However, it is widely known that the shear piezoresistance coefficient π_{44} for *n*-type bulk silicon vanishes to zero by using the conventional many-valley model of conduction band,^{15-17,23,24} where isoenergy surfaces of band energy in the vicinity of each valley in the reciprocal space are simple ellipsoids regardless of strain condition. Namely, Smith's experimental result for *n*-type silicon, $\pi_{44} = -13.8 \times 10^{-11} \text{ Pa}^{-1}$,¹ cannot be explained in terms of many-valley model with simple isoenergy ellipsoids, and one of the main causes of piezoresistive effect due to shear stresses is considered as a disorder of band-energy surface from the ellipsoids.^{25,26} The detail of band-energy surface can be simulated by first-principles calculations of bulk silicon models with some strains, so that

the estimate of the piezoresistive effect in terms of the first-principles electronic band structure is expected to be valid and useful.

In our previous work, we have presented an easy procedure to calculate the longitudinal and transverse piezoresistance coefficients in one-dimensional (1D) transport on the basis of first-principles electronic band structure of single-crystal doped silicon nanowire (SiNW) models.^{27,28} Unfortunately, the valence-band top of *p*-type bulk silicon cannot be represented by usual first-principles calculations because the spin-orbit interaction leading to the band split of the valence-band top is ignored, but our procedure used for SiNW models can be extended to three-dimensional (3D) transport in *n*-type bulk silicon for application to the shear piezoresistance coefficient as well as the longitudinal and transverse ones. In this paper, we simulated piezoresistance coefficients for *n*-type bulk silicon on the basis of first-principles electronic band structure in order to discuss the qualitative and quantitative precision of our procedure and to investigate physical origins of longitudinal, transverse, and shear piezoresistivity.

II. METHOD OF CALCULATION

We have carried out first-principles calculations of the periodic boundary models for single-crystal bulk silicon by FHI98MD program package,³⁷ based on the density-functional theory (DFT).³⁸ For the DFT exchange-correlation interaction, the generalized-gradient approximation (GGA) method was used with the Perdew-Burke-Ernzerhof (PBE) functional.³⁹ We adopted three-dimensional supercell approximation technique with norm-conserving pseudopotentials.

TABLE I. Strain tensors and calculated Poisson's ratios for bulk silicon models.

Model	Strain tensor	Poisson's ratio
[001] tensile	$\vec{\epsilon} = \begin{pmatrix} -\nu_{001}\epsilon_{001} & 0 & 0 \\ 0 & -\nu_{001}\epsilon_{001} & 0 \\ 0 & 0 & \epsilon_{001} \end{pmatrix}$	$\nu_{001}=0.25$
[110] tensile	$\vec{\epsilon} = \begin{pmatrix} (1-\nu'_{110})\epsilon_{110}/2 & (1+\nu'_{110})\epsilon_{110}/2 & 0 \\ (1+\nu'_{110})\epsilon_{110}/2 & (1-\nu'_{110})\epsilon_{110}/2 & 0 \\ 0 & 0 & -\nu_{110}\epsilon_{110} \end{pmatrix}$	$\nu_{110}=0.29$, ^a $\nu'_{110}=0.02$ ^b
[111] tensile	$\vec{\epsilon} = \begin{pmatrix} (1-2\nu_{111})\epsilon_{111}/3 & (1+\nu_{111})\epsilon_{111}/3 & (1+\nu_{111})\epsilon_{111}/3 \\ (1+\nu_{111})\epsilon_{111}/3 & (1-2\nu_{111})\epsilon_{111}/3 & (1+\nu_{111})\epsilon_{111}/3 \\ (1+\nu_{111})\epsilon_{111}/3 & (1+\nu_{111})\epsilon_{111}/3 & (1-2\nu_{111})\epsilon_{111}/3 \end{pmatrix}$	$\nu_{111}=0.14$
(001) shear	$\vec{\epsilon} = \begin{pmatrix} 0 & \epsilon_{\text{shear}}/2 & 0 \\ \epsilon_{\text{shear}}/2 & 0 & 0 \\ 0 & 0 & 0 \end{pmatrix}$	

^a[001] direction.^b[1 $\bar{1}$ 0] direction.

tials prepared according to the Hamann method.⁴⁰ The cutoff energy for wave functions of electrons with plane-wave expansion was set at 40 Ry (544 eV).

Conventionally, the first-principles calculations of *n*-type silicon semiconductors have been carried out with a doping atom such as phosphorus and arsenic, or an excess electron per unit cell, but these calculations should lead to an enormous overestimation of carrier concentration *N*. In this paper, we have calculated the first-principles band structures in the intrinsic semiconductor state. Treatment of the *n*-type semiconductor state will be discussed in Sec. III B.

The bulk silicon model was set as a general diamond-type primitive unit cell containing two silicon atoms, and we have optimized the cell parameters. We obtained the optimized cubic lattice constant of the diamond-type silicon crystal as $a_0=5.463$ Å at the level of our calculation. In addition, we have devised the [001], [110], and [111] uniaxial tensile models, and the (001) shear model. The effect of uniaxial tensile strain on structure with a Poisson's ratio was represented by partial optimization with a fixed lattice constant along the tensile direction with 0.1% tensile strain ($\epsilon=0.001$). The effect of shear strain was applied as a 0.1% in-plane simple shear strain on (001) plane without volume change. Components of strain tensor $\vec{\epsilon}$ and calculated Poisson's ratio ν for each model were determined as listed in Table I. Naturally, volume changes in tensile models due to 0.1% tensile strain are less than 0.1%, and the number of fast Fourier transformation grids in first-principle calculation was fixed at $30 \times 30 \times 30$ for all bulk silicon models. Therefore, the influence of the volume dependence on band energies can be almost disregarded.

The procedure to calculate piezoresistance coefficients follows our previous paper²⁷ for one-dimensional transport

in SiNW models. The essential points of the procedure are simple and adequate expression of the electronic state in the doped semiconductor state with a small amount of carrier occupation and treatment of effective masses in the one-dimensional style. We have extended the procedure to three-dimensional transport for applying the bulk silicon models. Detailed techniques shall be presented in following chapter.

III. RESULTS AND DISCUSSION

A. Deformation potentials for conduction band

First-principles calculated values of conduction-band bottom and valence-band top for each model are tabulated in Table II. In the conventional deformation-potential theory, the energy shift ΔE_c^α of valley α for an arbitrary homogeneous deformation has been represented with the strain tensor $\vec{\epsilon}$ and the deformation-potential constants Ξ_d and Ξ_u as follows:^{2,15,18,19}

$$\Delta E_c^\alpha = (\Xi_d \vec{1} + \Xi_u \{\mathbf{a}_\alpha \mathbf{a}_\alpha\}) : \vec{\epsilon}, \quad (1)$$

where $\vec{1}$ is the unit tensor, \mathbf{a}_α is a unit vector parallel to the reciprocal position vector of valley α , and braces $\{\}$ denote a dyadic product. Ξ_u represents the shift due to a shear deformation along the symmetry axis of the valley, while Ξ_d represents the shift due to a dilatation. The shift in the mean energy of the conduction-band extrema ΔE_c^0 is therefore written by

$$\Delta E_c^0 = \left(\Xi_d + \frac{1}{3} \Xi_u \right) \vec{1} : \vec{\epsilon}. \quad (2)$$

The quantity $\Xi_d + (1/3)\Xi_u$ is difficult to determine because the left side of Eq. (2) is derived from absolute band energies, but the shift in the mean energy gap,

TABLE II. Band energies of conduction-band bottom and valence-band top (in eV).

Band energies	Bulk silicon models				
	Strain-free	[001] tensile	[110] tensile	[111] tensile	(001) shear
Valleys on k_x axis	4.15251	4.14578	4.15106	4.14856	4.15296
Valleys on k_y axis	4.15251	4.14578	4.15106	4.14856	4.15296
Valleys on k_z axis	4.15251	4.15681	4.14416	4.14856	4.15306
Valence-band top at Γ point ^a	3.54025 (t)	3.53927 (d)	3.54021	3.53750	3.54402
		3.53047	3.53268	3.53334 (d)	3.53922
			3.53209		3.53776

^a(d) and (t), respectively, denote double and triple degeneracies.

$$\Delta E_g^0 = \left(\Xi_d + \frac{1}{3} \Xi_u - a \right) \vec{1} : \vec{\epsilon}, \quad (3)$$

can be easily introduced as a change in relative energies, where a is the deformation-potential constant for the shift in the mean energy of the valence-band extrema ΔE_v^0 as follows:

$$\Delta E_v^0 = a \vec{1} : \vec{\epsilon}. \quad (4)$$

The treatment of the strain Hamiltonian with the valence-band wave functions from the spin-orbit Hamiltonian shows that the value of ΔE_v^0 for three valence-band-top subbands is independent of the amount of the band split due to spin-orbit interaction,^{41,42} so that we have tried to evaluate the quantity $\Xi_d + (1/3)\Xi_u - a$ by use of band energies from regular first-principles calculations listed in Table II; $\Xi_d + (1/3)\Xi_u - a = 1.72, 2.18,$ and 2.07 eV under the [001], [110], and [111] tensile strains, respectively.

Furthermore, Ξ_u can be determined from the deviations of ΔE_c^α from ΔE_c^0 due to strain. Under uniaxial strain along [001] or [110] (i.e., $\epsilon_{xx} = \epsilon_{yy} \neq \epsilon_{zz}$), the deviations are given from Eqs. (1) and (2) by

$$\Delta E_c^\alpha - \Delta E_c^0 = \frac{2}{3} \Xi_u (\epsilon_{zz} - \epsilon_{xx}) = \frac{2}{3} \Xi_u (\epsilon_{zz} - \epsilon_{yy}) \quad (5)$$

for the valleys on k_z axis and

$$\Delta E_c^\alpha - \Delta E_c^0 = -\frac{1}{3} \Xi_u (\epsilon_{zz} - \epsilon_{xx}) = -\frac{1}{3} \Xi_u (\epsilon_{zz} - \epsilon_{yy}) \quad (6)$$

for those on k_x and k_y axes. Uniaxial strain along [111] keeps band energies of six valleys degenerate. We have calculated Ξ_u from band energies as 8.82 eV for the [001] tensile model and 8.85 eV for the [110] tensile model, respectively.

Experimental values of $\Xi_d + (1/3)\Xi_u - a$ and Ξ_u have been, respectively, reported to be 1.50 ± 0.30 and 8.6 ± 0.4 eV.³ For the quantity $\Xi_d + (1/3)\Xi_u - a$, the calculated value under the [001] tensile strain is consistent with the experimental one, but those under the [110] and [111] tensile strains seem to be overestimated. The reason for overestimate is considered that coupling effects between strain and spin-orbit interaction in the valence-band top have been perfectly ignored by regular first-principles calculations. On the contrary, our results of Ξ_u give good agreement with the

experimental values. Therefore, it is expected that deformation of the first-principles conduction band due to strain should lead to qualitative and quantitative estimates of piezoresistive properties for n -type bulk silicon.

B. Theory of carrier distribution and transport

In three-dimensional transport model for n -type semiconductor, the electrical resistivity can be generally represented as a 3×3 tensor in terms of carrier concentration and effective mass of the conduction band.⁴³ We have introduced the band carrier densities and their corresponding effective-mass tensors for each subband in the conduction band, and the electrical conductivity tensor \vec{G} or the reciprocal matrix of the resistivity tensor $\vec{\rho}$ has been added up over all subbands as follows:

$$\vec{G} = \vec{\rho}^{-1} = e^2 \sum_{j \in \text{CB}} n_j \vec{m}_j^{-* -1} \cdot \vec{\tau}_j, \quad (7)$$

where n_j is the j th conduction-band (CB) carrier electron density, \vec{m}_j^{-*} is the effective-mass tensor, $\vec{\tau}_j$ is the relaxation-time tensor, and e^2 is the square of the absolute value of the elementary electric charge. The band carrier densities are controlled by the Fermi energy E_F and temperature T ,

$$n_j = \frac{2}{V} \sum_{\mathbf{k}} w_{\mathbf{k}} \left[\exp\left(\frac{E_{j,\mathbf{k}} - E_F}{k_B T}\right) + 1 \right]^{-1}, \quad (8)$$

where $E_{j,\mathbf{k}}$ is the band energy of the j th subband at the \mathbf{k} point, $w_{\mathbf{k}}$ is the k -point weight for \mathbf{k} , V is the volume of the unit cell, and k_B is the Boltzmann constant. Due to an appropriate E_F , a total of conduction-band carrier electron densities should be equal to a total of valence-band hole densities in the intrinsic semiconductor state. Actual n -type semiconductors have a small quantity of carrier electrons, which must be much more than a quantity of holes, and we have defined the total number of carrier electrons per unit cell as δ ,^{27,28} which is a product of the carrier concentration N multiplied by the volume V and must be less by a few orders than 1. Under the condition that a small amount of the carrier occupation in n -type semiconductor state does not cause significant changes in the band structure, δ can be given by an appropriate upward shift in the Fermi energy updated to E_F as follows:

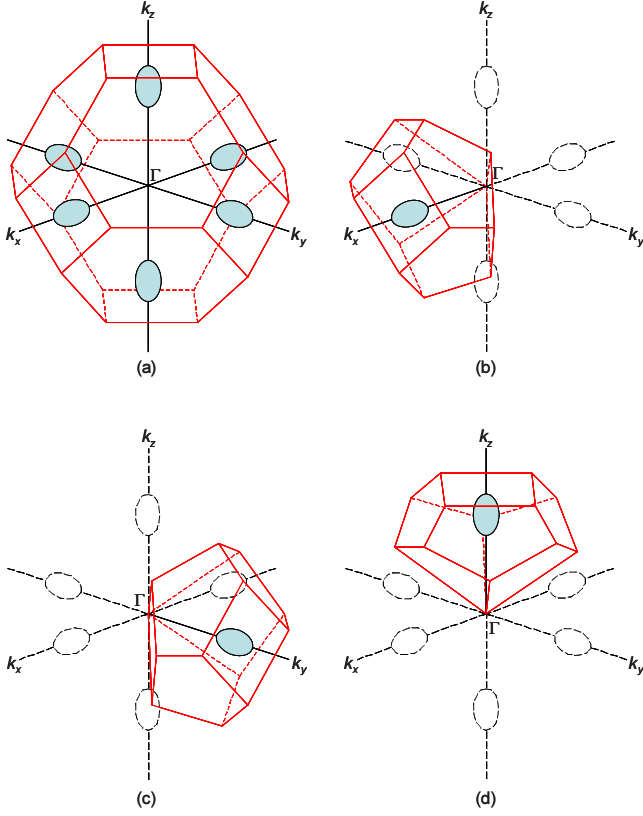


FIG. 1. (Color online) Images of the reciprocal space for the bulk silicon model: (a) the first Brillouin zone and the valley regions (b) v_1 for the valley on $+k_x$ axis, (c) v_3 for the valley on $+k_y$ axis, and (d) v_5 for the valley on $+k_z$ axis.

$$\delta = NV = 2 \sum_{j \in \text{CB}} \sum_{\mathbf{k}} w_{\mathbf{k}} \left[\exp\left(\frac{E_{j,\mathbf{k}} - E'_F}{k_B T}\right) + 1 \right]^{-1}, \quad (9)$$

where the set of $\{E_{j,\mathbf{k}}\}$ is identical to that in the intrinsic semiconductor state. We have set δ to an appropriate constant less than 10^{-2} , and then E'_F in n -type carrier occupations have been solved according to Eq. (9).

For the many-valley conduction band of bulk silicon, the first Brillouin zone (BZ) can be divided into six valley regions $\{v_\alpha\}$ that contain a valley bottom, respectively, as shown in Fig. 1. Properties on the right hand of Eq. (7) are replaced by the regional ones as follows:

$$\vec{G} = \vec{\rho}^{\leftarrow-1} = e^2 \sum_{j \in \text{CB}} \sum_{v_\alpha} n_{j,\alpha} \vec{m}_{j,\alpha}^{\leftrightarrow-1} \cdot \vec{T}_{j,\alpha}, \quad (10)$$

where the regional carrier electron density in v_α can be defined as

$$n_{j,\alpha} = \frac{2}{V} \sum_{\mathbf{k} \in v_\alpha} w_{\mathbf{k}} \left[\exp\left(\frac{E_{j,\mathbf{k}} - E'_F}{k_B T}\right) + 1 \right]^{-1}, \quad (11)$$

with the updated E'_F determined by δ in Eq. (9). Practically, the summation over all subbands in the conduction band can be replaced by the summation of only two subbands; the lowest subband of multivalley ($j=\text{MV}$) and the second lowest subband minimized at X points, on the boundary of the first BZ, due to the noncrossing rule ($j=\text{NC}$).⁴⁴ As long as

we are aware, there is no previous article with considering the NC subband for piezoresistive effect of n -type bulk silicon. The carrier occupations on the third lowest and higher subbands can be regarded as zero because they are quite fewer than that of the NC subband.

The effective mass is generally also given by a 3×3 tensor. The reciprocal effective-mass tensor of the subband j in v_α is defined as⁴⁵

$$\vec{m}_{j,\alpha}^{\leftrightarrow-1} = \frac{1}{\hbar^2} \mathbf{R} \begin{pmatrix} \frac{\partial^2 E_j}{\partial k_x^2} & \frac{\partial^2 E_j}{\partial k_x \partial k_y} & \frac{\partial^2 E_j}{\partial k_x \partial k_z} \\ \frac{\partial^2 E_j}{\partial k_y \partial k_x} & \frac{\partial^2 E_j}{\partial k_y^2} & \frac{\partial^2 E_j}{\partial k_y \partial k_z} \\ \frac{\partial^2 E_j}{\partial k_z \partial k_x} & \frac{\partial^2 E_j}{\partial k_z \partial k_y} & \frac{\partial^2 E_j}{\partial k_z^2} \end{pmatrix} \mathbf{R}^T, \quad (12)$$

at the k point of band energy minimum in v_α , where \hbar is equal to Planck's constant divided by 2π , and \mathbf{R} is the three-dimensional rotation matrix from the principal axes of cubic lattice. For the relaxation times tensor in silicon systems, strict or complicated formulas have recently been presented by some research groups.^{4,20,46–48} In this paper, we have presented the approximation that all of the band relaxation times are isotropic and, furthermore, are equal and constant regardless of stress. This step seems to be rough to some extent, but the variation rate of carrier conductivity can be easily and adequately represented in consideration of the canceling of almost part of band relaxation times.

For calculations of the Fermi energy shift in Eq. (9) and the regional electron carrier densities in Eq. (11), we have performed a sampling within the first BZ according to the three-dimensional Gauss-Legendre quadrature. Concretely, we have carried out the triple-loop adaptation of the Gauss-Legendre quadrature⁴⁹ of $n=29$ in $[0, b_0]$ ($b_0=2\pi/a_0$) for an eighth of the first BZ where $k_x, k_y,$ and k_z are all positive, and sampling points of the quadrature in the exterior of the first BZ, i.e., $k_x+k_y+k_z > (3/2)b_0$, have been omitted. The reason why we have selected $n=29$ is that the set of sampling \mathbf{k} points contains very close points to the conduction-band extrema. For other seven eighths of the first BZ, the same scheme has been applied with a corresponding integral space. The regional integral of Eq. (11) has been calculated by use of same sampling points for Eq. (9) in the interior and boundaries of the valley region. Values of sampling points on boundary faces or lines have been shared equally with related regions.

Numerical results of the regional electron carrier densities $n_{j,\alpha}$ on some conditions for carrier concentration and temperature are displayed in Fig. 2. In the strain-free and [111] tensile models, carrier electrons are always distributed equivalently to six regions, so that $(n_{\text{MV},\alpha} + n_{\text{NC},\alpha})/N$ is equal to $1/6$ for each α regardless of concentration and temperature. On the contrary, the distributions of carrier electrons in the [001] and [110] tensile models are uneven, originated from the band deformation due to strain in Eqs. (5) and (6). Occupation ratio $n_{\text{NC},\alpha}/N$ can be regarded as zero in low temperature, and the summation of occupation ratios on the NC subband is less than 0.3% even at $T=373$ K. However,

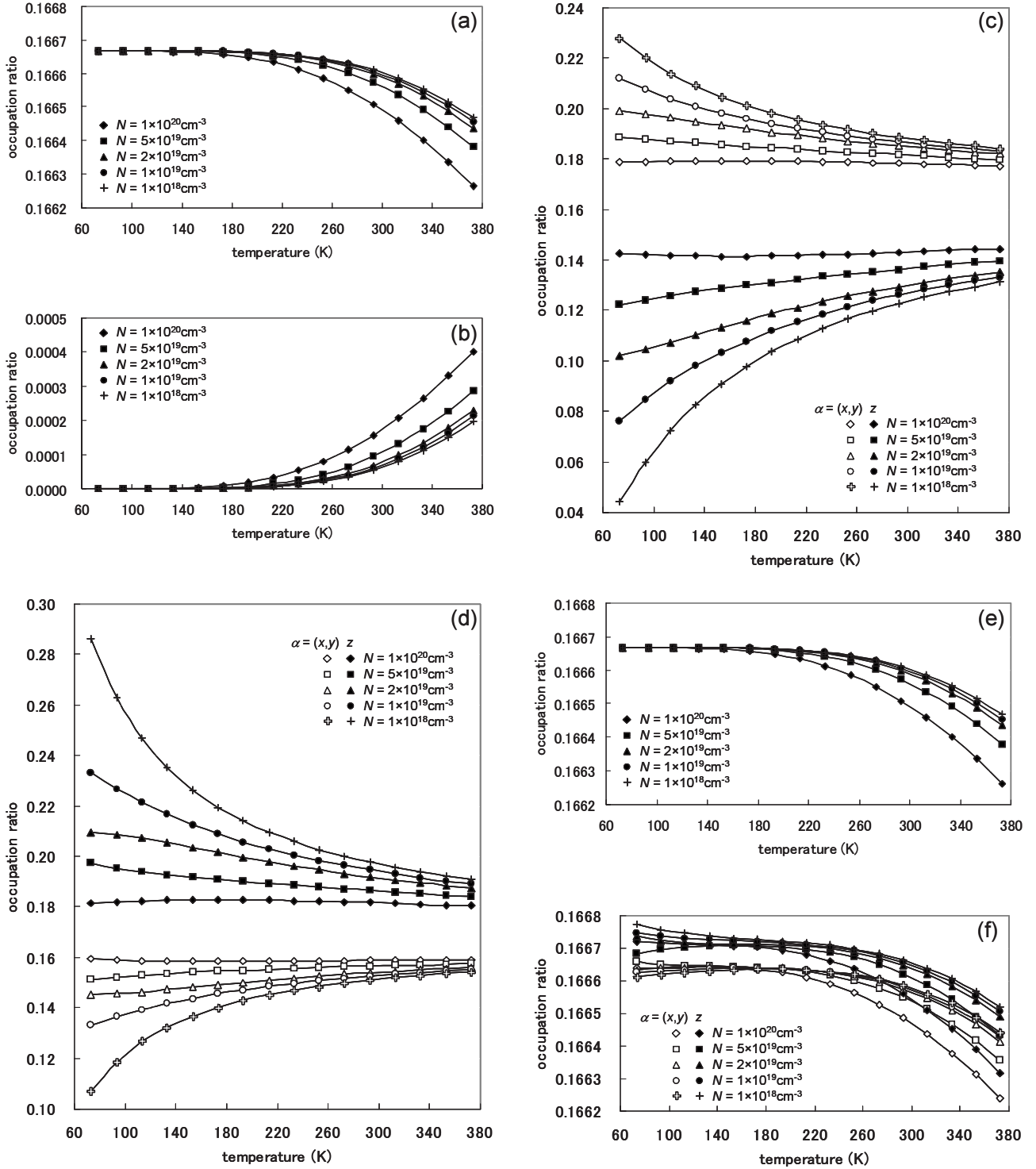


FIG. 2. Variation of carrier occupation ratios with temperature: (a) $n_{MV,\alpha}/N$ in the strain-free model, (b) $n_{NC,\alpha}/N$ in the strain-free model, (c) $n_{MV,\alpha}/N$ in the [001] tensile model, (d) $n_{MV,\alpha}/N$ in the [110] tensile model, (e) $n_{MV,\alpha}/N$ in the [111] tensile model, and (f) $n_{MV,\alpha}/N$ in the (001) shear model. $n_{NC,\alpha}/N$ in the strain and shear models are similar values as that in the strain-free model. $\alpha=x$ means v_1 and v_2 , $\alpha=y$ means v_3 and v_4 , and $\alpha=z$ means v_5 and v_6 .

we have judged that a consideration of the NC subband for analysis of the piezoresistivity is indispensable because the change in the effective masses for the NC subband due to strain is incredibly large.

The diagonal elements of the reciprocal effective-mass tensor in Eq. (12) have been obtained at $\mathbf{k}_{j,\alpha}^{\min}$, the k point of

band-energy minimum, from the second derivative of the band-energy curve function with respect to the reciprocal space axes after operation of the rotation matrix \mathbf{R} , where the band-energy curve function was a quartic function derived by least-squares fitting of band energies with the interval of $0.0005b_0$ in $[k_{j,\alpha}^{\min} - 0.025b_0, k_{j,\alpha}^{\min} + 0.025b_0]$. For $j=NC$, the

TABLE III. Diagonal elements of reciprocal effective-mass tensors $\partial^2 E_j / \partial k_i^2$ for subband $j=$ MV and NC for each orientation of coordinate axes (in m_0^{-1} , inverse of electron rest mass).

$j=$ MV	Regions v_1 and v_2		Regions v_3 and v_4		Regions v_5 and v_6	
	Strain-free	[001] tensile	Strain-free	[001] tensile	Strain-free	[001] tensile
k_i						
[100]	1.0292	1.0451	5.1140	5.1213	5.1140	5.1132
[010]	5.1140	5.1213	1.0292	1.0451	5.1140	5.1132
[001]	5.1140	5.1192	5.1140	5.1192	1.0292	1.0403
k_i						
[110]	3.0721	3.0758	3.0721	3.0758	5.1170	5.1630
[001]	5.1140	5.2755	5.1140	5.2755	1.0292	1.0416
[1 $\bar{1}$ 0]	3.0721	3.0798	3.0721	3.0798	5.1170	5.0755
k_i						
[111]	3.7537	3.7738	3.7537	3.7738	3.7537	3.7738
[1 $\bar{1}$ 0]	3.0721	3.0814	3.0721	3.0814	5.1170	5.0914
[11 $\bar{2}$]	4.4326	4.4197	4.4326	4.4197	2.3957	2.4125
$j=$ NC	Regions v_1 and v_2		Regions v_3 and v_4		Regions v_5 and v_6	
	Strain-free	[001] tensile	Strain-free	[001] tensile	Strain-free	[001] tensile
k_i						
[100]	1.4796	1.4840	4.7415	4.7398	4.7415	4.7451
[010]	4.7415	4.7398	1.4796	1.4840	4.7415	4.7451
[001]	4.7415	4.7350	4.7415	4.7350	1.4796	1.4785
k_i						
[110]	3.2692	10.3457	3.2692	10.3457	8.6939	0.7815
[001]	4.7415	4.6999	4.7415	4.6999	1.4796	25.5680
[1 $\bar{1}$ 0]	3.2692	10.3689	3.2692	10.3689	8.6939	8.6979
k_i						
[111]	3.8756	18.9844	3.8756	18.9844	3.8756	18.9844
[1 $\bar{1}$ 0]	3.2692	19.8432	3.2692	19.8432	8.6939	8.7015
[11 $\bar{2}$]	4.5395	16.8602	4.5395	16.8602	2.6824	20.0238

least-squares fitting has been performed in $[k_{j,\alpha}^{\min} - 0.025b_0, k_{j,\alpha}^{\min}]$ if the band-energy curve function contains a singular effect due to the noncrossing rule at $\mathbf{k}_{j,\alpha}^{\min}$.⁴⁴ These diagonal elements of the reciprocal effective-mass tensor for each orientation of coordinate axes are shown in Table III. The off-diagonal elements can be derived from the diagonal elements for another orientation with operating a proper rotation matrix. Details will be discussed in Sec. III D.

To summarize, our treatment of carrier distribution and transport includes some distinguishing characteristics not seen in earlier methods: arbitrary control of total carrier concentration owing to an appropriate shift in the Fermi energy, finite integral procedure based on the region partitioning of the first BZ corresponding to the multivalley model, and consideration of the change in the effective masses for the NC

subband. They have supported the quality and quantity of our simulation.

C. Longitudinal and transverse piezoresistance coefficients

Under the uniaxial tensile stress σ along one of the orthogonal coordinate axes due to the matrix \mathbf{R} , the longitudinal piezoresistance coefficient π_l and transverse one π_t are, respectively, defined as

$$\pi_l = \frac{\Delta\rho_l}{\rho_0\sigma}; \quad \pi_t = \frac{\Delta\rho_t}{\rho_0\sigma}, \quad (13)$$

where ρ_0 is the average value of resistivities along the three orthogonal coordinate axes, that is, a third of the trace of the

resistivity tensor $\vec{\rho}$ without stress, and $\Delta\rho_{l,t}$ are, respectively, variations in resistivity for parallel and vertical directions to the uniaxial tensile stress as follows:

$$\Delta\rho_{l,t} = \rho_{l,t} - \rho_0 = \frac{1}{G_{l,t}^{\text{tensile}}} - \rho_0, \quad (14)$$

where $G_{l,t}^{\text{tensile}}$ are diagonal elements of the conductivity tensor for the tensile model \vec{G}^{tensile} . The uniaxial tensile stress has been represented by a linear-response approximation according to the classical Hooke's law, $\sigma = Y\epsilon$, with Young's modulus Y and tensile strain ϵ . From the viewpoint of strain, π_l and π_t are also, respectively, given by

$$\pi_l = \frac{K_l}{Y}; \quad \pi_t = \frac{K_t}{Y}, \quad (15)$$

where $K_{l,t}$ are the longitudinal and transverse strain gauge factors defined as

$$K_{l,t} = \frac{\Delta\rho_{l,t}}{\rho_0\epsilon}. \quad (16)$$

In this paper, the value of ϵ is 0.001 for all uniaxial tensile models as mentioned above, and the temperature dependence of $K_{l,t}$ has been computed without any empirical parameter by means of the procedure presented in Sec. III B. On the contrary, since Young's modulus originates in properties of Si-Si bonds, the temperature dependence of Y should be hard to evaluate exactly unless dynamical analysis such as first-principles molecular-dynamics calculation has been performed. The temperature dependence of elastic moduli has already been clarified by use of enormous experimental data, and we have referred to temperature dependence of the elastic stiffness constants $c_{ij}(T)$ of bulk silicon by Varshni's formula,⁵⁰

$$c_{ij}(T) = c_{ij}^0 - s/\{\exp(t/T) - 1\}, \quad (17)$$

where $c_{ij}^0 = 167.5018$ GPa, $s = 5.32972$ GPa, and $t = 407.0$ K for $c_{11}(T)$; $c_{ij}^0 = 65.0079$ GPa, $s = 2.31036$ GPa, and $t = 334.8$ K for $c_{12}(T)$; $c_{ij}^0 = 80.0735$ GPa, $s = 2.24966$ GPa, and $t = 497.4$ K for $c_{44}(T)$, and Young's moduli for each orientation can be written by

$$Y_{001}(T) = \frac{(c_{11} - c_{12})(c_{11} + 2c_{12})}{c_{11} + c_{12}}, \quad (18)$$

$$Y_{110}(T) = 2 \left[\frac{c_{11}}{(c_{11} - c_{12})(c_{11} + 2c_{12})} + \frac{1}{2c_{44}} \right]^{-1}; \quad (19)$$

$$Y_{111}(T) = 3 \left(\frac{1}{c_{11} + 2c_{12}} + \frac{1}{c_{44}} \right)^{-1}. \quad (20)$$

π_l and π_t are represented by three primitive piezoresistance coefficients π_{11} , π_{12} , and π_{44} in terms of the Euler rotation as follows:^{23,24}

$$\pi_l = \pi_{11} - 2(\pi_{11} - \pi_{12} - \pi_{44})(l_1^2 m_1^2 + m_1^2 n_1^2 + n_1^2 l_1^2); \quad (21)$$

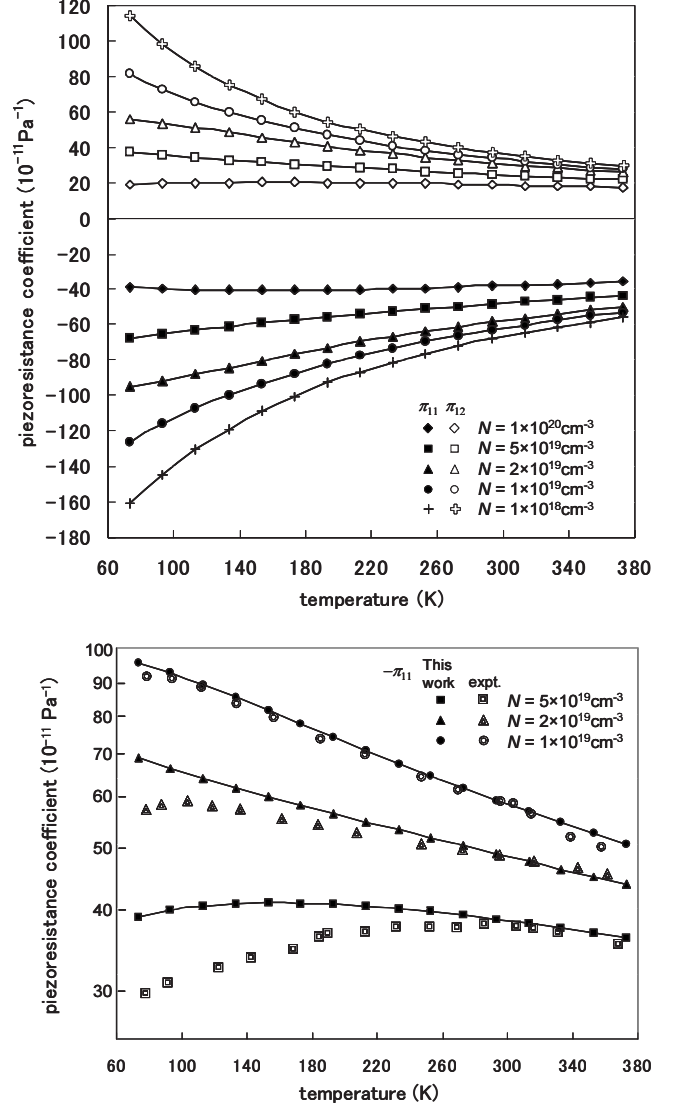


FIG. 3. Variation of π_{11} (closed symbols) and π_{12} (open symbols) with temperature in *n*-type silicon derived from the [001] tensile stress. Additional logarithmic graph shows $-\pi_{11}$ with experimental values (double symbols) reported by Tufte and Stelzer. (Ref. 5)

$$\pi_t = \pi_{12} + (\pi_{11} - \pi_{12} - \pi_{44})(l_2^2 l_2^2 + m_1^2 m_2^2 + n_1^2 n_2^2), \quad (22)$$

where (l_1, m_1, n_1) and (l_2, m_2, n_2) are direction cosines according to uniaxial stress and vertical directions, respectively.

We can define the theoretical values of π_{11} and π_{12} simply as the computational values of π_l and π_t for the [001] tensile strain, respectively, through Eqs. (21) and (22). Figure 3 shows π_{11} and π_{12} calculated from Eq. (15) with respect to temperature and carrier concentration, and they give qualitatively good agreement with the experimental values.^{1,5,6} In particular, our results of π_{11} are in beautiful agreement with experimental value by Tufte and Stelzer⁵ on the order of 10^{19} cm^{-3} carrier concentration. The behaviors of π_{11} and π_{12} are clearly reflected by that of the regional electron carrier densities in Fig. 2(c), because the mobilities or the

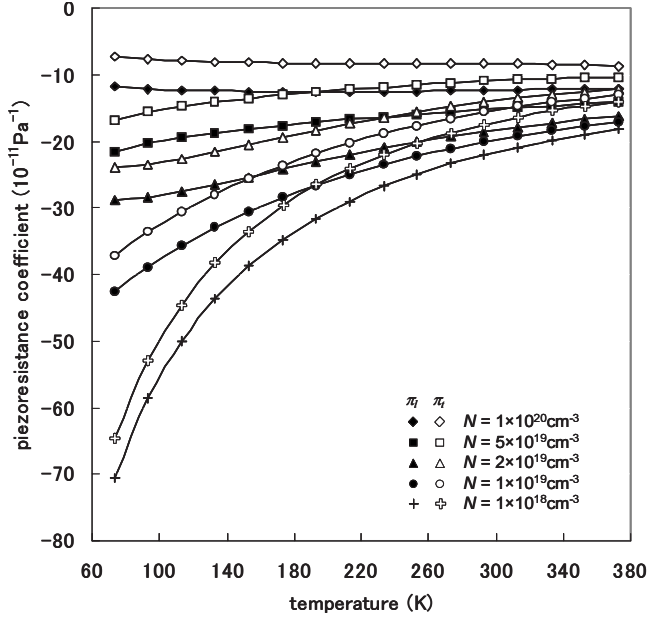


FIG. 4. Variation of π_l (closed symbols) and π_t (open symbols) for the [110] tensile stress in the (001) plane with temperature in n -type silicon.

effective-mass tensors for six valleys hardly change with respect to the [001] uniaxial stress as shown in Table III. To summarize, π_{11} and π_{12} originate from the energy gap between the valleys of the MV subband, and therefore, they are vividly dependent on temperature and carrier concentration.

For the [110] tensile model, the computational values of π_l and π_t on the (001) plane are displayed in Fig. 4. Both of π_l and π_t are obtained as negative values as known experimentally. The computational values of π_l and π_t on the (112) plane for the [111] tensile model are shown in Fig. 5. The carrier occupation ratio is independent of the [111] tensile stress, so that the change in conductivity is perfectly due to the variations of mobilities for valleys. As a result, both of π_l and π_t for the [111] tensile strain are very small, but the variations of mobilities for the NC subband affect π_l and π_t sensitively in high temperature.

D. Shear piezoresistance coefficient

In terms of Eqs. (21) and (22), the primitive shear piezoresistance coefficient π_{44} should be equal to $\pi_l - \pi_t$ for both the (001) plane of the [110] tensile model and any plane of the [111] tensile model. Values of π_{44} calculated from the [110] and [111] tensile models, respectively, are shown in Fig. 6. We can reproduce the important experimental result that π_{44} should be a negative value.

Furthermore, in this paper, we have tried to calculate the primitive shear piezoresistance coefficient π_{44} directly by the work of shear stress τ . For the (001) shear model along the principal axes, the shear piezoresistance coefficient π'_{66} , which is equal to π_{44} , is defined as

$$\pi'_{66} = \frac{\Delta\rho_6}{\rho_0\tau}, \quad (23)$$

where $\Delta\rho_6$ is a variation in ρ_{xy} , the off-diagonal element of the resistivity tensor $\vec{\rho}$ corresponding to the plane affected by

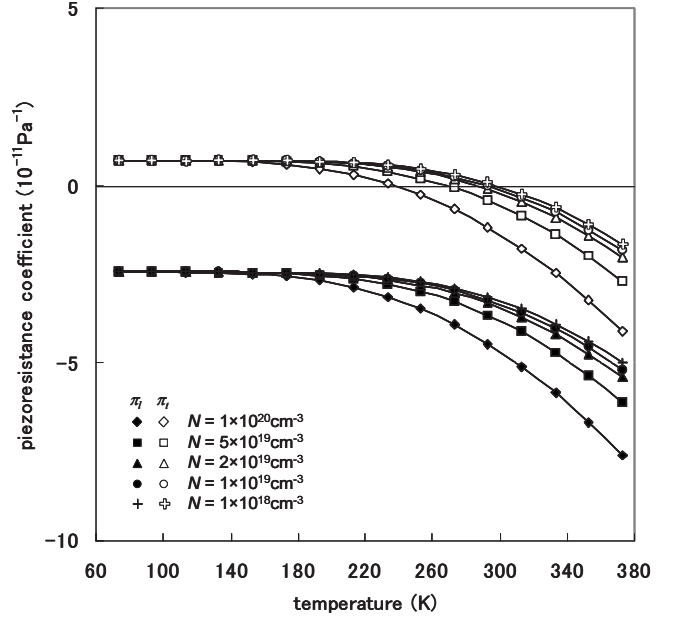


FIG. 5. Variation of π_l (closed symbols) and π_t (open symbols) for the [111] tensile stress in the (112) plane with temperature in n -type silicon.

τ . Similarly as π_l and π_t , the gauge factor expression has been introduced for π_{44} by

$$\pi_{44} = \frac{K_{\text{shear}}}{c_{44}} \quad (24)$$

with the classical Hooke's law $\tau = c_{44}\epsilon$, where the shear gauge factor

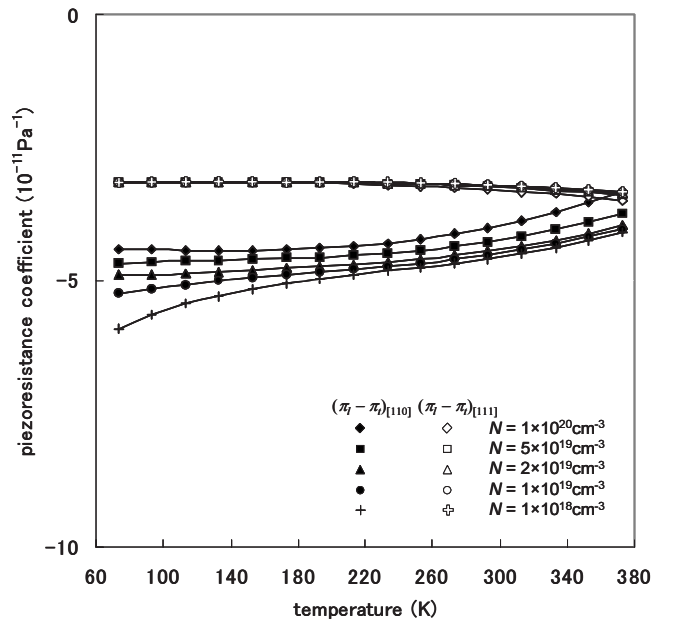


FIG. 6. Variation of $\pi_l - \pi_t$ with temperature with temperature in n -type silicon derived from the [110] tensile stress in the (001) plane (closed symbols) and the [111] tensile stress in the (112) plane (open symbols).

TABLE IV. Diagonal and nondiagonal elements of reciprocal effective-mass tensors for subband j =MV and NC in the (001) shear model (in m_0^{-1} , inverse of electron rest mass).

j =MV	v_1 and v_2	v_3 and v_4	v_5 and v_6
$\partial^2 E_{MV} / \partial k_x^2$	1.0398	5.1158	5.1180
$\partial^2 E_{MV} / \partial k_y^2$	5.1158	1.0398	5.1180
$\partial^2 E_{MV} / \partial k_u^2$	3.0775	3.0775	5.1598
$\partial^2 E_{MV} / \partial k_v^2$	3.0771	3.0771	5.0777
$\partial^2 E_{MV} / \partial k_x k_y$	0.0002	0.0002	0.0411
j =NC	v_1 and v_2	v_3 and v_4	v_5 and v_6
$\partial^2 E_{NC} / \partial k_x^2$	8.5294	4.7437	4.7493
$\partial^2 E_{NC} / \partial k_y^2$	4.7437	8.5294	4.7493
$\partial^2 E_{NC} / \partial k_u^2$	10.9455	10.9455	0.7817
$\partial^2 E_{NC} / \partial k_v^2$	11.0094	11.0094	8.7074
$\partial^2 E_{NC} / \partial k_x k_y$	-0.0319	-0.0319	3.9628

$$K_{\text{shear}} = \frac{\Delta\rho_6}{\rho_0\epsilon} \quad (25)$$

has been computed without any empirical parameter with shear strain $\epsilon=0.001$. $\Delta\rho_6$ can be represented with components of the conductivity tensor for the (001) shear model \vec{G}^{shear} as follows:

$$\Delta\rho_6 = -\frac{G_{xy}^{\text{shear}}}{G_{xx}^{\text{shear}}G_{yy}^{\text{shear}} - (G_{xy}^{\text{shear}})^2}. \quad (26)$$

According to Eqs. (10) and (12), G_{xy}^{shear} is derived from the nondiagonal element of the reciprocal effective-mass tensor, where the second derivative of the band-energy $\partial^2 E_j / \partial k_x \partial k_y$ can be written by

$$\frac{\partial^2 E_j}{\partial k_x \partial k_y} = \frac{1}{2} \left(\frac{\partial^2 E_j}{\partial k_u^2} - \frac{\partial^2 E_j}{\partial k_v^2} \right) \quad (27)$$

with $k_u=2^{-1/2}(k_x+k_y)$ and $k_v=2^{-1/2}(k_x-k_y)$. The second derivatives with respect to k_u and k_v were, respectively, calculated from quartic functions by least-squares fitting mentioned above. The values of elements of the reciprocal effective-mass tensor in the (001) shear model are tabulated in Table IV.

The temperature dependence of c_{44} has been adopted from Eq. (17), and then, π_{44} in Eq. (24) with respect to temperature and carrier concentration are shown in Fig. 7. At the room temperature $T=300$ K, we have obtained π_{44} in the range of $-4.3 \times 10^{-11} \text{ Pa}^{-1}$ ($N=1 \times 10^{20} \text{ cm}^{-3}$) to $-4.5 \times 10^{-11} \text{ Pa}^{-1}$ ($N=1 \times 10^{18} \text{ cm}^{-3}$). The primitive shear piezoresistance coefficient π_{44} due to the direct π_{66}' calculation hardly dependent on temperature and concentration, and almost accords with $\pi_{44}s$ from the [110] and [111] tensile models shown in Fig. 6. The effect of the NC subband in high temperature observed in Fig. 5 is almost vanished.

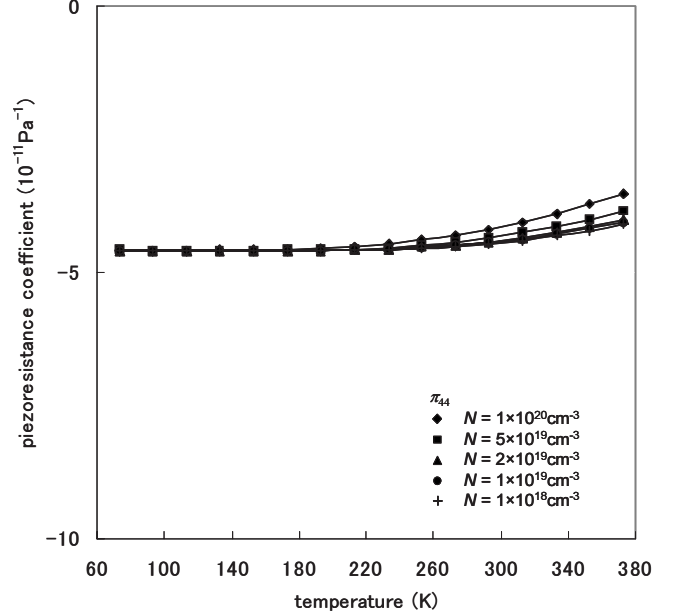


FIG. 7. Variation of π_{44} with temperature with temperature in *n*-type silicon derived from the (001) shear stress.

As listed in Table IV, we have found that the effect of (001) shear strain on the band-energy surface of the MV and NC subbands is localized at the valleys on k_z axis in v_5 and v_6 regions. The distortion of isoenergy ellipsoids in the vicinity of the valleys of the conduction band due to the shear strain has been discussed before.^{25,26} We shall clarify the behavior of band-energy surface around the valleys on k_z axis due to the (001) shear strain. We cannot apparently recognize the distortion of band-energy surface of $E_{MV}(\mathbf{k})$ due to the shear strain as shown in Fig. 8(a), but the difference of the band energy between the strain-free and (001) shear models shown in Fig. 8(b) gives contours like simple hyperbolas, $k_x'k_y'=\text{const}$, where $k_x'=k_x-k_x^{\text{min}}$ and $k_y'=k_y-k_y^{\text{min}}$. This contour plot is in accord with the suggestion by Kanda and Suzuki that the band energy in the vicinity of $\mathbf{k}^{\text{min}}(\equiv\mathbf{k}_{MV,5}^{\text{min}})$ can be written with strain ϵ_{xy} as^{25,26}

$$E_{MV}(\mathbf{k}) = \frac{\hbar^2(k_x'^2 + k_y'^2)}{2m_{\perp}} + A\hbar^2\epsilon_{xy}k_x'k_y' + \frac{\hbar^2(k_z - k_z^{\text{min}})^2}{2m_{\parallel}} \quad (28)$$

where m_{\perp} and m_{\parallel} are diagonal elements of effective-mass tensor, and A is a proper constant. The local curvature $(1/\hbar^2)\partial^2 E_{MV}/\partial k_r^2$ of the MV band-energy surface at $\mathbf{k}(k_r, \theta) = (k_x', k_y', k_z^{\text{min}}) = (k_r \cos \theta, k_r \sin \theta, k_z^{\text{min}})$ in v_5 is simply given by $1/m_{\perp} + A\hbar^2\epsilon_{xy} \sin 2\theta$ for $E_{MV}(\mathbf{k})$ written by Eq. (28), that is, it is a constant when $\epsilon_{xy}=0$.

However, isoenergy surfaces for the MV subband in the vicinity of each valley are not simple ellipsoids even in the strain-free model. Figures 8(c) and 8(d), respectively, show the local curvature for the strain-free model and the (001) shear model. The local curvature is almost constant along the parallel direction to k_x and k_y axes, but it is reduced along the

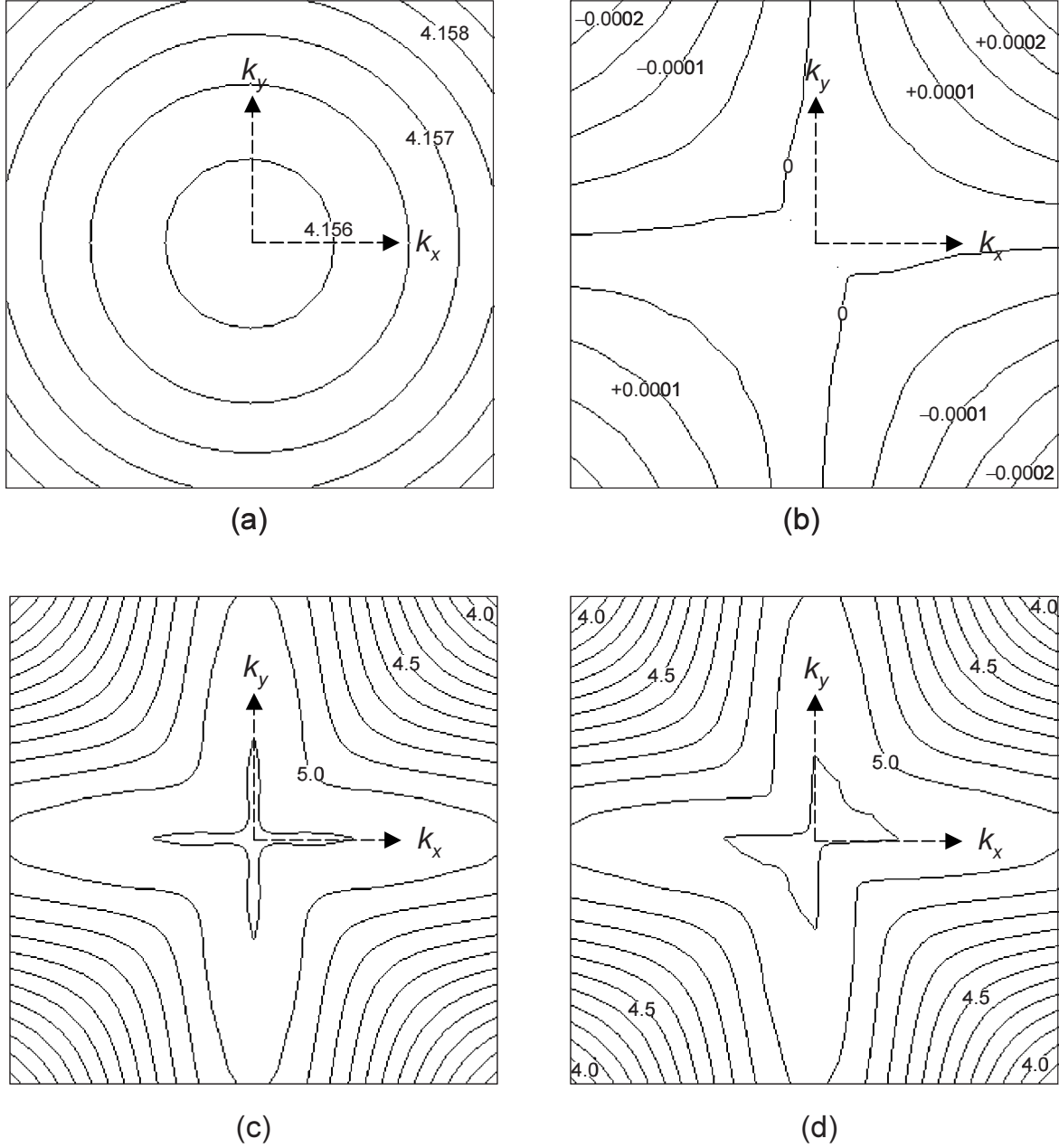


FIG. 8. Contour plots of band-energy surface analyses around the valley in region v_5 for the MV subband: (a) band-energy surface of the (001) shear model in eV, (b) difference of band energy $\{E_{MV}^{\text{shear}}(\mathbf{k}) - E_{MV}^{\text{shear}}(\mathbf{k}^{\text{min}})\} - \{E_{MV}^{\text{free}}(\mathbf{k}) - E_{MV}^{\text{free}}(\mathbf{k}^{\text{min}})\}$ in eV, and (c) and (d) the local curvatures of the strain-free and the (001) shear models, respectively, in m_0^{-1} . The map is located on the plane $k_z = k_z^{\text{min}}$ with $0.05b_0 \times 0.05b_0$ square and the map center of each map is $(k_x^{\text{min}}, k_y^{\text{min}})$.

oblique direction as being off \mathbf{k}^{min} . In the (001) shear model, it seems that the degree of this deviation from a simple ellipsoid along the oblique direction is affected by the shear strain, and as a result, contours like $k'_x k'_y = \text{const}$ are observed in the difference of the band energy between the strain-free and (001) shear models as shown in Fig. 8(b).

IV. CONCLUSION

We have simulated the piezoresistance coefficients in n -type single-crystal bulk silicon on the basis of first-principles electronic band structure. The conduction-band

diagram by our calculations of the primitive unit cell with two silicon atoms for bulk silicon gives appropriate deformation potentials for tensile strains, leading to qualitative and quantitative estimates of piezoresistive properties for n -type bulk silicon. The n -type semiconductor state has been represented by an appropriate upward shift in the Fermi energy in the intrinsic semiconductor state, and the carrier conductivity has been calculated using band carrier densities and their corresponding effective-mass tensors derived from the first-principles band diagram. Our simple procedure to calculate the piezoresistance coefficients for a small carrier concentration is valid qualitatively and quantitatively for electron

transport in the multivalley conduction-band structure of *n*-type bulk silicon; π_{11} and π_{12} originate from the energy gap between the valleys, whereas π_{44} arises from a distortion of the deviation from isoenergy ellipsoids in the valleys of the conduction band, and can be presented clearly as a negative constant. The distinction between the origins of longitudinal, transverse, and shear piezoresistivity can be followed as a dependence on a carrier concentration or temperature. It is expected that the procedure to calculate the piezoresistance

coefficients in this paper can be applied to other semiconductor systems.

ACKNOWLEDGMENTS

This work was partly conducted under the “Highly Integrated, Complex MEMS Production Technology Development Project” sponsored by the New Energy and Industrial Technology Development Organization (NEDO), for which the authors express their gratitude.

*Present address: Research Institute for Nanomachine System Technology, Ritsumeikan University, Kusatsu, Shiga 525–8577, Japan; koichi-a@st.ritsumeiki.ac.jp

- ¹C. S. Smith, *Phys. Rev.* **94**, 42 (1954).
- ²F. H. Pollak and M. Cardona, *Phys. Rev.* **172**, 816 (1968).
- ³L. D. Laude, F. H. Pollak, and M. Cardona, *Phys. Rev. B* **3**, 2623 (1971).
- ⁴J. F. Creemer and P. J. French, *J. Appl. Phys.* **96**, 4530 (2004).
- ⁵O. N. Tufte and E. L. Stezler, *Phys. Rev.* **133**, A1705 (1964).
- ⁶O. N. Tufte and E. L. Stezler, *J. Appl. Phys.* **34**, 313 (1963).
- ⁷O. N. Tufte, P. W. Chapman, and D. Long, *J. Appl. Phys.* **33**, 3322 (1962).
- ⁸K. Yamada, M. Nishihara, S. Shimada, M. Tanabe, M. Shimazoe, and Y. Matsuoka, *IEEE Trans. Electron Devices* **29**, 71 (1982).
- ⁹B. Borchert and G. E. Dorda, *IEEE Trans. Electron Devices* **35**, 483 (1988).
- ¹⁰A. T. Bradley, R. C. Jaeger, J. C. Suhling, and K. J. O’Connor, *IEEE Trans. Electron Devices* **48**, 2009 (2001).
- ¹¹M. L. Lee and E. A. Fitzgerald, *J. Appl. Phys.* **94**, 2590 (2003).
- ¹²T. Toriyama and S. Sugiyama, *Sens. Actuators, A* **108**, 244 (2003).
- ¹³W. Zhao, J. He, R. E. Belford, L.-E. Wernersson, and A. Sea-baugh, *IEEE Trans. Electron Devices* **51**, 317 (2004).
- ¹⁴S. E. Thompson, G. Sun, Y. S. Choi, and T. Nishida, *IEEE Trans. Electron Devices* **53**, 1010 (2006).
- ¹⁵R. W. Keyes, *Solid State Phys.* **11**, 149 (1960).
- ¹⁶C. Herring, *Bell Syst. Tech. J.* **34**, 237 (1955).
- ¹⁷C. Herring and E. Vogt, *Phys. Rev.* **101**, 944 (1956).
- ¹⁸I. Balslev, *Phys. Rev.* **143**, 636 (1966).
- ¹⁹C. G. Van de Walle and R. M. Martin, *Phys. Rev. B* **34**, 5621 (1986).
- ²⁰M. V. Fischetti and S. E. Laux, *J. Appl. Phys.* **80**, 2234 (1996).
- ²¹H. Hasegawa, *Phys. Rev.* **129**, 1029 (1963).
- ²²S. Richard, F. Aniel, G. Fishman, and N. Cavassilas, *J. Appl. Phys.* **94**, 1795 (2003).
- ²³W. G. Pfann and R. N. Thurston, *J. Appl. Phys.* **32**, 2008 (1961).
- ²⁴Y. Kanda, *IEEE Trans. Electron Devices* **29**, 64 (1982).
- ²⁵Y. Kanda and K. Suzuki, *Phys. Rev. B* **43**, 6754 (1991).
- ²⁶Y. Kanda, *Sens. Actuators, A* **28**, 83 (1991).
- ²⁷K. Nakamura, Y. Isono, and T. Toriyama, *Jpn. J. Appl. Phys.* **47**, 5132 (2008).
- ²⁸K. Nakamura, Y. Isono, T. Toriyama, and S. Sugiyama, *Jpn. J. Appl. Phys.* **48**, 06FG09 (2009).
- ²⁹Y. Kanda, *Sens. Actuators* **4**, 199 (1983).
- ³⁰Y. Kanda, *Jpn. J. Appl. Phys.* **26**, 1031 (1987).
- ³¹K. Matsuda, K. Suzuki, K. Yamamura, and Y. Kanda, *J. Appl. Phys.* **73**, 1838 (1993).
- ³²M. Bao and Y. Wang, *Sens. Actuators* **12**, 49 (1987).
- ³³Y. Ohmura, *Phys. Rev. B* **42**, 9178 (1990).
- ³⁴P. Kleimann, B. Semmache, M. Le Berre, and D. Barbier, *Phys. Rev. B* **57**, 8966 (1998).
- ³⁵E. X. Wang, P. Matagne, L. Shifren, B. Obradovic, R. Kotlyar, S. Cea, M. Stettler, and M. D. Giles, *IEEE Trans. Electron Devices* **53**, 1840 (2006).
- ³⁶K. Seeger, *Semiconductor Physics, An Introduction*, 6th ed. (Springer-Verlag, Heidelberg, 1989), pp. 10–33.
- ³⁷M. Bockstedte, A. Kley, J. Neugebauer, and M. Scheffler, *Comput. Phys. Commun.* **107**, 187 (1997).
- ³⁸P. Hohenberg and W. Kohn, *Phys. Rev.* **136**, B864 (1964).
- ³⁹J. P. Perdew, K. Burke, and M. Ernzerhof, *Phys. Rev. Lett.* **77**, 3865 (1996).
- ⁴⁰D. R. Hamann, *Phys. Rev. B* **40**, 2980 (1989).
- ⁴¹G. Dresselhaus, A. F. Kip, and C. Kittel, *Phys. Rev.* **98**, 368 (1955).
- ⁴²S. Zwerdling, K. J. Button, B. Lax, and L. M. Roth, *Phys. Rev. Lett.* **4**, 173 (1960).
- ⁴³C. Kittel, *Introduction to Solid State Physics*, 8th ed. (Wiley, New York, 2005), p. 200.
- ⁴⁴C. Kittel, *Introduction to Solid State Physics*, 8th ed. (Wiley, New York, 2005), p. 177.
- ⁴⁵J. M. Ziman, *Principle of the Theory of Solids*, 2nd ed. (Cambridge University Press, New York, 1972), pp. 183–186.
- ⁴⁶T. Kinoshita, K. M. Itoh, M. Schadt, and G. Pensl, *J. Appl. Phys.* **85**, 8193 (1999).
- ⁴⁷S. Jin, Y. J. Park, and H. S. Min, *J. Appl. Phys.* **99**, 123719 (2006).
- ⁴⁸T. Markussen, R. Rurali, M. Brandbyge, and A.-P. Jauho, *Phys. Rev. B* **74**, 245313 (2006).
- ⁴⁹F. B. Hildebrand, *Introduction to Numerical Analysis* (McGraw-Hill, New York, 1956), pp. 323–325.
- ⁵⁰Y. P. Varshni, *Phys. Rev. B* **2**, 3952 (1970).